

Locating inhomogeneities in tissue by using the most probable diffuse path of light

Jing Bai

Tianxin Gao

Kui Ying

Tsinghua University
Department of Biomedical Engineering
Beijing, China, 100084
E-mail: deabj@tsinghua.edu.cn

Nanguang Chen

National University of Singapore
Bioengineering Division & ECE
Department Faculty of Engineering
Singapore 117576

Abstract. Characterization of human tissue using near-IR (NIR) light is becoming increasingly popular. The light signal transmitted from the tissue contains information concerning inhomogeneities in tissue, such as size, position, and pathological states (benign or malignant). We discuss the most probable diffuse path (MPDP) related to frequency-domain diffuse photon density waves (DPDWs) propagating inside turbid media. We find that for a medium of finite size, the existence of boundaries between tissue and nonscattering media would have considerable impact on the path shape. It is also demonstrated that such paths can be used to obtain higher accuracy in localizing absorbers embedded in a homogeneous background. Based on the proposed MPDP, a new method for 3-D localization of heterogeneities in turbid media is proposed, which is validated by experiments using Intralipid and pork fat. The experiments are performed with an NIR breast cancer detection system designed and assembled in our lab, using 780-nm NIR light. In Intralipid, when the size of a single absorber is less than 1 cm, the localization error is about 2 mm. The results from pork fat are also acceptable. © 2005 Society of Photo-Optical Instrumentation Engineers. [DOI: 10.1117/1.1896968]

Keywords: most probable diffuse path; diffuse photon density waves; frequency domain; near infrared; optical imaging; breast cancer.

Paper 03109 received Aug. 21, 2003; revised manuscript received Feb. 19, 2004; accepted for publication Oct. 13, 2004; published online Apr. 29, 2005.

1 Introduction

Recently, the interest in applying near-IR (NIR) light in clinical diagnosis has greatly increased among researchers around the world due to the characteristics of the NIR light. One major characteristic of the NIR light is that it is nonionizing to human tissues within a tissue window ranging from 600 (limited by the very strong absorption of hemoglobin) to 1000 nm (limited by the significant water absorption). In this wavelength range, the NIR light penetrates human tissues more easily than at other wave bands. NIR light can be used to differentiate between soft tissues due to their different absorption or scattering characteristics at different NIR wavelengths. In addition, natural chromophores (such as oxyhemoglobin) have a specific ability of absorption, which makes it possible to obtain functional images. The strong absorption of the NIR light in human tissues may explain the appearance of hemorrhage, tumor, or high oxygen saturation of blood. The spectroscopic information is important in studies of brain functions and breast cancer. Locating the absorber in the human body may be helpful in locating the positions of the tumor or

the hemorrhagic spot. However, how to accurately locate an absorber has become a challenging but very worthwhile issue.

Recently, much work has been published¹⁻⁸ to discuss the use of rf-modulated NIR light in detecting inhomogeneities inside turbid media. The goal of this work was to develop noninvasive methods to diagnose human breast cancer in its early stage. However, biological organs, e.g., the breast, generally have similar dimensions. The existing boundaries caused by the biological organs have a significant impact on the propagation of diffuse photon density waves (DPDWs) inside a medium, and thus on the received signals. For simplicity, some previous works used quite large phantoms.² Some other works used highly symmetrical geometry, such as cylinders.³⁻⁵ Among these works, the calculation of Green's function was relatively simple and the computation time was reduced. In reality, however, the situation is more complicated. A nonsymmetrical model may be more practical to better describe the real situation. Therefore, in this paper we proposed a new algorithm to include the nonsymmetrical property. This can help us better understand the real characteristics of DPDW propagation.

Address all correspondence to Dr. Jing Bai, Tsinghua University, Department of Electrical Engineering, Institute of Biomedical Engineering, Beijing 10084 China. E-mail: deabj@tsinghua.edu.cn

In this paper, we first derive the most probable diffuse path (MPDP) in the frequency domain for a transmission mode from the diffusion equation. Second, we present a new method for locating absorbers in turbid media. Third, we describe experiments and results. Finally, we discuss some issues arisen from this work.

2 Methods

2.1 Diffusion Equation and the MPDP

Perelman et al. treated the propagation of light in a turbid medium as a free random walk.^{9–11} They used the path integral with a quasiparticle Lagrangian to find the most probable trajectory, or classical path, over which photons can be found. Their theory can also be expressed as follows: for the given initial and final states and transport time, the probability density of finding a photon at the most probable path is maximized. As we see here, the most probable trajectory was apparently described in the time domain.

In reality, compared with the time-domain (TD) measurements, the frequency-domain (FD) method is simpler and more reliable in terms of data interpretation and immunity from noise. Medical FD equipment is more economical and portable.¹² More attention is currently being paid to the FD method. Therefore, in our work, we defined the MPDP in the FD.

In the framework of wave optics, energy transfer is along the gradient direction of the density of electromagnetic energy. However, energy transfer can also be described by the classical movement of particles in the framework of geometrical optics. Therefore, we use the same two frameworks to describe our defined quasiparticle, i.e., the particle, which represents the average effect of wave progress at the macroscale.

The diffusion equation is described in detail later, as the basis of our theory.

Light propagation is usually described by diffusion approximation in a highly scattering medium, when the source frequency is¹³ less than 1 GHz. In the FD, according to the diffusion approximation, the flux vector $\mathbf{j}(\mathbf{r}, \omega)$ can be expressed¹⁴ as the gradient of fluence rate $\Phi(\mathbf{r}, \omega)$:

$$\mathbf{j}(\mathbf{r}, \omega) = -D\nabla\Phi(\mathbf{r}, \omega), \quad (1)$$

with

$$D = \frac{1}{3[(1-g)\mu_s + \mu_a]} = \frac{1}{3(\mu_a + \mu'_s)},$$

where D is the diffusion coefficient, \mathbf{r} is the location, and ω is the modulation frequency. Anisotropy factor g is the mean cosine of the scattering angle, written as $g = \langle \cos \theta \rangle$; μ_a is the absorption coefficient; μ_s is the scattering coefficient; and μ'_s is the reduced scattering coefficient, defined as $\mu'_s = \mu_s(1 - g)$.

Equation (1) represents a proportional relationship between the macroscopic flow of the scattering particles and the spatial distribution of the particle density, which is analogous to the flow conservation law of fluid dynamics. Substituting Eq. (1) into the radiative transfer equation⁷ (RTE), the RTE can be simplified as the diffusion equation, written as

$$(\nabla^2 + k^2)\Phi(\mathbf{r}, \omega) = -\frac{1}{cD}S(\mathbf{r}, \omega), \quad (2)$$

in the FD, where k denotes the complex wave number,

$$k \equiv -i \left(\frac{\mu_a c - i\omega}{Dc} \right)^{1/2}, \quad (3)$$

$S(\mathbf{r}, \omega)$ is the source item representing the source energy intensity, and c is the speed of light in the media. In an infinite homogeneous medium, the DPDW excited by a sinusoidally modulated source at the original point propagates as a spherical wave.¹⁵

$$\Phi(\mathbf{r}, \omega)\exp(i\omega t) = \frac{S}{4\pi cDr} \exp(-ikr)\exp(i\omega t), \quad (4)$$

where S is the amplitude of the source intensity, and r is the distance between the observed point and the original point.

The DPDW described by Eq. (4) is a new type of wave used to describe the random migration of diffuse photons in turbid media. The properties of the DPDW are different from those of general waves, such as sound and light waves. For general waves, the square of their amplitude is of the order of the magnitude of energy density, while the amplitude of DPDW itself is of the order of the magnitude of energy density. The field variables of the general wave are represented by complex numbers in the FD, but the energy density and flux are real numbers, while the energy density and flux of DPDW are complex numbers. What we are interested in is the propagation of information carried by the alternating component of energy current.

For convenience of calculation, we use $\mathbf{j}_{\text{info}}(\mathbf{r}, \omega)$ to take the place of $\mathbf{j}(\mathbf{r}, \omega)$ in Eq. (1). We consider the amplitude of $\Phi(\mathbf{r}, \omega)$, thus $\mathbf{j}_{\text{info}}(\mathbf{r}, \omega)$ becomes

$$\mathbf{j}_{\text{info}}(\mathbf{r}, \omega) = -D\nabla\{\text{sqrt}[\Phi^*(\mathbf{r}, \omega)\Phi(\mathbf{r}, \omega)]\}, \quad (5)$$

where $\Phi^*(\mathbf{r}, \omega)$ is the conjugate of $\Phi(\mathbf{r}, \omega)$. The direction of $\mathbf{j}_{\text{info}}(\mathbf{r}, \omega)$ represents the direction along which quasiparticles move. The direction of the movement of quasiparticles is useful to determine the MPDP of photons in a turbid medium.

Usually in FD method, light sources are modulated with sine waves of a single frequency. In this paper, we define the ac components of the fluence rate and flux with respect to a fixed angular frequency. Note that a dc component always exists accompanying the ac component (for the light source intensity, fluence rate, detected flux, and so on). However, we are only interested in the ac component (more specifically, the amplitude of the ac component) in this paper.

As we mentioned earlier, Perelman et al. first introduced the concept of the most probable trajectory (or classical path) in their work. Here in our work, we propose the most probable path in the steady state. In the steady state, for the given distribution of the fluence rate, and the injection point and exit point (or start and end point) the MPDP is defined as the path on which a scattered photon is most likely to occur. For each point on the MPDP, the direction of MPDP is the direction of the flux vector of this point. The MPDP can be considered as a random walk process from the injection point to the exit

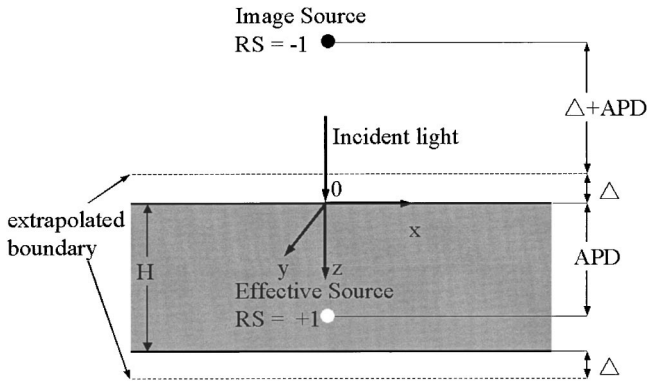


Fig. 1 The 2-D tissue model and the boundary conditions.

point. The step length is the transport mean free path, determined by $l_{tr}=3D$. The moving direction at point \mathbf{r} is determined by $\mathbf{j}_{info}(\mathbf{r},\omega)$ in Eq. (5).

Our definition of the most probable path in the FD does not come from photon trajectories, and is different from the TD approach. Instead, we start directly from the diffusion equation and try to localize the most important energy (information) flow carried by the diffusive photon density waves across the turbid media. Such localization is represented by the trajectory of a conceptual quasiparticle, which is not a real particle at all.

Now we must calculate the MPDP in a transmission mode for a medium with finite thickness, since the transmission mode is frequently adopted for breast cancer diagnosis.

Before giving our model, we recall the well-accepted semi-infinite model first. For a semi-infinite turbid medium, the perpendicularly incident light can be replaced by an effective source and an image source.^{16,17} The effective source is an isotropic point source located an APD (average penetration depth) into the medium. The image source is the image of the effective source by the extrapolated boundary. If we let the residual strength (RS) of the effective source be 1, then the RS of the image source will be -1 .

For the transmission mode, the thickness of tissue is an important factor, i.e., the medium we studied must have at least one finite dimension, e.g., the Z direction. For simplicity, in the MPDP calculation, we assume that the quasiparticle travels in the X-Z plane. This is the MPDP in two dimensions. From Fig. 1, we can see that the 2-D model is infinity in the X direction, while the thickness in the Z direction is defined as H . As shown in Fig. 1, the light enters into the medium from the original point along the Z direction. There are two extrapolated boundaries in our model, which is different with the half-infinite model.

In our model, image method¹⁶ is used to construct a fluence rate solution that satisfies $\Phi(x,z=-\Delta)=0$ and $\Phi(x,z=H+\Delta)=0$. The two extrapolated boundaries work like two mirrors. For the effective source with the unit strength at $(0,APD)$, there are infinitely many image sources created by the two extrapolated boundaries at $[x=0, z=2N(H+2\Delta) \pm (\Delta+APD)-\Delta]$, where N is an integer. Figure 1 shows the 2-D tissues model and the boundary conditions with $N=0$. Different N s give different image sources. In Fig. 1, Δ is the extrapolation distance. We chose $\Delta=APD=l_{tr}$ during

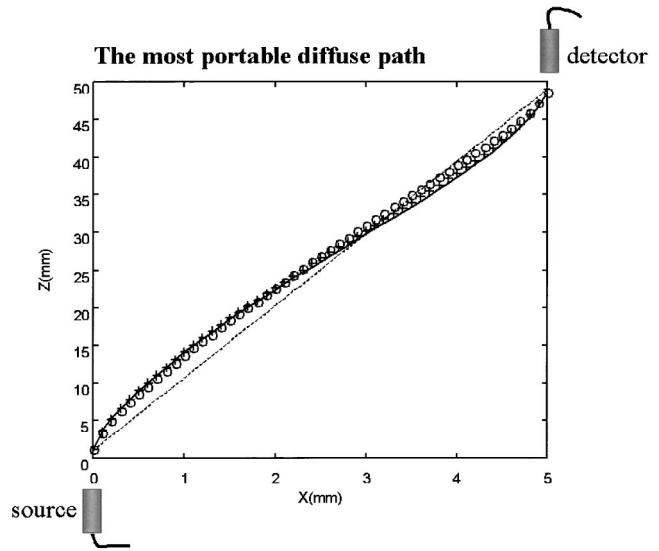


Fig. 2 MPDP at different modulation frequencies. Solid line: dc; +: 50 MHz; O: 200 MHz. A dashed straight line is also plotted for comparison.

calculation.¹⁷ Although the image sources are at infinity, only the first 10 to 20 terms are mainly used. The contribution of the other image sources is greatly diminished by the far distance.

According to Eq. (4), we can calculate the 2-D distribution of fluence rate in a 3-D medium by superposing the fluence rate of DPDWs generated by the effective source and image sources. Then the calculated fluence rate is substituted into Eq. (5) and the flux vector in the 2-D area can be obtained. First, a vertically injecting quasiparticle comes to $(0,l_{tr})$. Second, the vertically injecting quasiparticle will randomly take an initial angle and move to the next step. The step length is always l_{tr} . The following points in the medium follow the direction of $\mathbf{j}_{info}(\mathbf{r},\omega)$ given by Eq. (5). When the quasiparticle is close enough to the surface, i.e., less than l_{tr} to the surface, the path will end at the surface of the medium, either on top or at the bottom. The path ending at the detection point is the one we require. The MPDP is affected by several factors: μ_a, μ'_s , the refractive index n, H , the modulation frequency ω of the source, and the relative position between the source and the detector, defined as the lateral distance dx . From our model, the MPDP we calculate is not the analytic function of the trajectory, but a series of points on it. Therefore, for the convenience of calculation, a polynomial is created from these points to describe the MPDP. The function $z = f(x, \mu_a, \mu'_s, n, H, dx, \omega)$ is used to describe the polynomial, abbreviated as $z = f(x)$.

Figure 2 shows one example of the transmitting MPDP. The source is at $(X,Z)=(0,0)$, while the detector is at $(5,50)$ (the units are millimeters). The parameters are $\mu_a = 0.005 \text{ mm}^{-1}$, $\mu'_s = 1 \text{ mm}^{-1}$, $n = 1.33$, $H = 50 \text{ mm}$, and $dx = 5 \text{ mm}$. When $f = 49.86 \text{ MHz}$, the MPDP can be described by a polynomial as

$$Z = P(1)X^N + P(2)X^{(N-1)} + \dots + P(N)X + P(N+1),$$

$$N = 10,$$

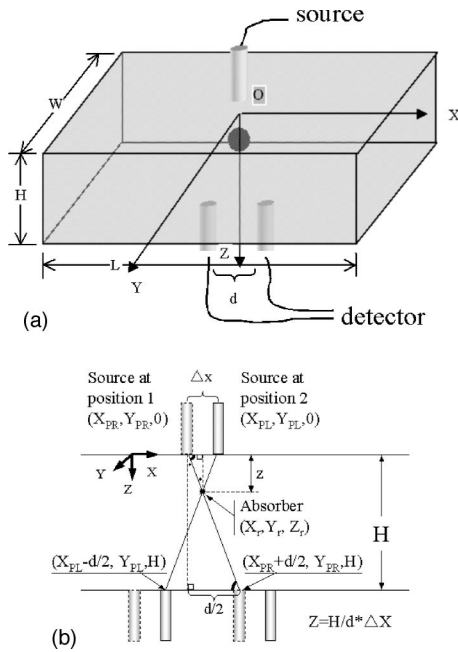


Fig. 3 Locating the absorber in three dimensions with the MPDP: (a) localization system in transmission mode and (b) MPDP shown by a straight line.

where $P = \{0.0013 \quad -0.0335 \quad 0.3725 \quad -2.3342 \quad 9.0375 \dots$
 $-22.2446 \quad 34.4206 \quad -31.6160 \quad 14.5160 \quad 8.2596 \quad 0.9408\}$

The calculated MPDP takes on an S shape. The symbols “○” and “+,” and the solid lines show the path at different source frequencies: 200 MHz, 50 MHz, and 0 Hz (the direct current condition), respectively. From Fig. 2 we can see that the higher the source frequency, the closer is the path to a straight line. The straight dotted line represents the direct line between the source and the detector.

2.2 Localization of Inhomogeneities Using MPDP

Generally a projection method is useful to detect the inhomogeneities in tissue, e.g., a mammogram is a projection of the breast in film. The NIR light source can also be used to make a projection of breast tissue,¹⁸ referred to as optical mammography. However, optical mammography can acquire depth information concerning breast tissue, while conventional mammogram, x-ray mammography, cannot. This is because that the projection data of the NIR light are obtained by the point-to-point scanning of a source-detector pair. The projection data thus represent the information in a matrix of the sampling points. By using some reconstruction methods, the depth information concerning the breast tissue can be obtained.

In our work, we propose a method with the MPDP in the steady state to locate an absorber in three dimensions, which includes determining the depth information of the absorber. Figures 3(a) and 3(b) are used to describe our method in three and two dimensions, respectively. We use L , W , and H to represent the length, width, and height of the medium, respectively; and d is the distance between the two detectors. For simplicity and to describe our method, we assume in Fig. 3 that the MPDP is a straight line between the source and the detector. In Fig. 3(b) there are one source and two detectors in the plane parallel to the X - Z plane, which means the source-

detector triangle is always in the plane parallel to the X - Z plane. In this example, the source is at $(x_s, y_s, 0)$, the left detector is at $(x_s - d/2, y_s, H)$, and the right detector is at $(x_s + d/2, y_s, H)$. At $y = 0$, the source-detector triangle scans the first row along the X direction. Then y is increased by an incremental, the source-detector triangle scans the second row along the X direction. This processes goes on until the last y is reached, and the whole scanning area has been scanned. When the source and detectors scan the sample, the absorber will shut out the light twice at position 1 (dashed lines) and position 2 (solid lines). At position 1 ($X_{PR}, Y_{PR}, 0$), the source, the absorber, and the right detector are in one straight line, and the right detector shows an absorption peak. At position 2 ($X_{PL}, Y_{PL}, 0$), the source, the absorber, and the left detector are in one straight line, and the left detector shows an absorption peak.

After scanning in the X - Y plane, two optical projections are obtained from the two detectors respectively; each has a shadow of the absorber. Ideally, the absorber center of the left projection is at (X_{PL}, Y_{PL}) , and the right projection is at (X_{PR}, Y_{PR}) . We assume that the projection coordinate system is the same as the source coordinate system. When the source is at $(X_{PL}, Y_{PL}, 0)$ and $(X_{PR}, Y_{PR}, 0)$, respectively, there are two MPDPs that pass through the absorber and end at the left detector $(X_{PL} - d/2, Y_{PL}, H)$ and the right detector $(X_{PR} + d/2, Y_{PR}, H)$, respectively. The question is how to reconstruct the real coordinates [defined as (X_r, Y_r, Z_r)] of the absorber from the absorber centers in the projection image, i.e., (X_{PL}, Y_{PL}) and (X_{PR}, Y_{PR}) . According to the geometry of the source-detector triangle Y_{PL} should be equal to Y_{PR} in theory, and X_r should be in the middle of X_{PL} and X_{PR} . Considering the system error, the average of Y_{PL} and Y_{PR} will be used as Y_r :

$$X_r = (X_{PL} + X_{PR})/2, \quad (6)$$

$$Y_r = (Y_{PL} + Y_{PR})/2, \quad (7)$$

$$\Delta X = |X_{PL} - X_{PR}|, \quad (8)$$

where ΔX is the distance between the two positions of the source [see Fig. 3(b)]. Equations (6) and (7) are universal, no matter whether the MPDP is a straight line or an S-shaped curve. In Fig. 3(b), where the MPDP is a straight line, the depth of the absorber can be easily obtained as

$$\frac{Z}{\Delta X/2} = \frac{H}{d/2}, \quad (9)$$

$$Z = \frac{H}{d} \Delta X.$$

For the S-shaped MPDP, we plug $\Delta X/2$ into the polynomial function mentioned earlier to obtain the depth of absorber:

$$Z = f(\Delta X/2). \quad (10)$$

Finally, we summarize the procedure that is used to locate the absorber with the MPDP.

1. Step 1. Scan the detected area point by point and acquire two projections for each point in the scanning matrix.
2. Step 2. Locate the absorber centers $[(X_{PL}, Y_{PL})$ and $(X_{PR}, Y_{PR})]$ in the projection images.
3. Step 3. Calculate the coordinates of the real absorber center (X_r, Y_r) using Eqs. (6) and (7).
4. Step 4. Calculate the depth of the real absorber center by using Eqs. (8) and (10). Here Eq. (10) is the MPDP function obtained in Sec. 2.1.

2.3 Image Processing

After scanning we can acquire two data matrices, referred to as \mathbf{M}_L and \mathbf{M}_R . Each of the matrices has N (in the X direction, $N=9$) $\times M$ (in the Y direction, variable) points. The subscript L represents the detector at the “left” side of source and R represents the “right.” The notation $M_L(i, j)$ represents the element in the line i and column j of the matrix of the left projection, and i represents the ordinal of the source along the X direction and j represents the step in the Y direction.

To improve the resolution in the X direction, we combined \mathbf{M}_L and \mathbf{M}_R to make one matrix \mathbf{M} . The following equations describes how to combine the two matrices:

$$\mathbf{M}(2i-1, j) = \frac{M_L(i, j) + M_R(i, j)}{2}, \quad 1 \leq i \leq 8,$$

$$\mathbf{M}(2i, j) = \frac{M_L(i+1, j) + M_R(i, j)}{2}, \quad 1 \leq i \leq 8.$$

The image of the combined matrix \mathbf{M} has a better resolution than that of each individual matrix \mathbf{M}_L and \mathbf{M}_R . This was validated by our experiments.

The image segmentation method is also used to improve the resolution of the image. Set a threshold and reset the pixels with a value that is less than the threshold. The nonzero part will be isolated by the reset pixels, so different parts of the image will be partitioned, i.e., segmented. It is important, but sometimes hard to choose the threshold.

It has been found that, in the image of diffuse light amplitude, the blurring level of the absorbers’ edge is associated with the depth of absorbers. For absorbers in the middle level of tissue, a threshold close to the absorption peak should be chosen.

The combination method and the segmentation method make the shadow of the absorbers clearer, which is helpful in finding the size and shape of the absorbers with more accu-

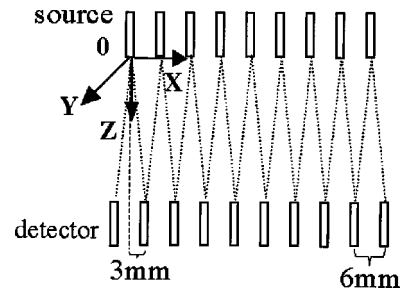


Fig. 4 Sources and detectors.

racy. The results of using these two methods were shown by the combined image and the deblurred image, respectively.

All the imaging and reconstruction functions used in this paper were developed in the Matlab 5.3 environment.

2.4 Experiment

Based on our theory, we developed a prototype in our lab. The prototype was designed to detect breast tumor. The 780-nm NIR light generated by laser diode (Sharp Co. LT027) was modulated at 49.86 MHz and carried by an optical fiber bundle to the surface of the sample. The optical fiber bundles also conduct the signal to photomultiplier tubes (Hamamatsu R928). To implement the detection method described in Sec. 2.2, the prototype has 19 optical fiber bundles in total. As shown in Fig. 4, 9 of them in one row are the light sources, while the other 10 in another row are detectors. They work as nine groups of source-detector triangles, as shown in Fig. 3. The nine groups are arranged in one row along the X direction in the plane vertical to the Y axis. The distance of the adjacent groups is 6 mm and the lateral distance between source and detector (dx) in each group is 3 mm. An electrical switch took the place of a mechanical scan, which can save time. Nine sources lit alternately just like the source moved along the X axis in 6-mm steps. At one time, only one source was lit and two detectors (nearest to the lit source) received the signal. The inner diameter of each fiber bundle is 2 mm. Using the prototype, the amplitude information of the penetrating light was detected and used to image and reconstruct.

In our experiments, Intralipid and pork were used to simulate breast tissues. Tumors often absorb more lights than normal tissues, so a black plastic ball or some fictile objects of different shapes and sizes or muscle (from pork) were used to simulate them. The imaging area was 45 mm wide (in the X direction) and 57 mm long (in the Y direction). The coordinate system used here was the same as the coordinate system de-

Table 1 Single absorber experiments in Intralipid.

No.	Absorber	Real Coordinates (X, Y, Z)	Distance to the Surface	Reconstruction Coordinates (X_r, Y_r, Z_r)	Error (x, y, z)
1	8-mm ball	(10,20,15)	15	(9.4,20.6,16.8)	(0.6,0.6,1.8)
2	8-mm ball	(10,25,30)	20	(9.8,24.4,33.1)	(0.2,0.6,3.1)
3	Cylinder*	(21,27,35)	15	(23.0,27.6,34.5)	(2.0,0.6,0.5)

*The cylinder is 5 mm long, and 2 mm in diameter. (Units are millimeters).

Table 2 Experiments of an absorber pair in Intralipid (units are millimeters).

No.	Absorber	Real Coordinates (X, Y, Z)	Distance to the Surface	Reconstruction Coordinates (X_r, Y_r, Z_r)	Error (x, y, z)
4	1	(15,30,15)	15	(22.4,30.4,13.2)	(0.1,0.4,1.8)
	2	(30,30,15)	15		
5	1	(25,27,26)	24	(31.5,26.7,27.8)	(1.0,0.3,1.8)
	2	(40,27,26)	24		

scribed in Figs. 3 and 4. The $z=0$ point was on the top surface of the phantom. The initial position of the first light source (the first source from the left in Fig. 4) was used as the original point in the X - Y plane in each experiment.

During the experiments, the scan area was kept in the center of the phantom, about 10 mm away from the nearest edge. The absorbers were also kept at least 10 mm away from the edges of the phantom.

2.4.1 Experiment with Intralipid

We put 0.9% Intralipid ($\mu_a = 0.005 \text{ mm}^{-1}$, $\mu'_s = 1 \text{ mm}^{-1}$) into a transparent plastic box, which was 140 mm long and 73 mm wide. The solution was 50 mm deep. A black plastic ball (8 mm in diameter) and a black cylinder (5 mm long and 2 mm in diameter) were used as the absorbers.

Experiments 1 to 3 used one single absorber, but at different depths of the solution, as shown in Table 1.

Experiments 4 and 5 used a pair of absorbers in different position in the solutions, as shown in Table 2. The absorber pair contained two black balls (8 mm in diameter). The distance between them was 15 mm. The sources and detectors were arranged along the X direction. To test the resolution of the source-detector triangle the two balls were in one line parallel to the X axis. In experiment 4, the absorber pair was 15 mm away from the surface, while in experiment 5, the absorber was 24 mm from the surface, as shown in Table 2.

More experiments were performed to compare the reconstruction accuracy of the MPDP with that of the straight line. In each experiment, the 8-mm-diam black ball was put at a different depth of the solution. The real depth of the absorber (Z_{org}) was changed from 5 to 45 mm with a 5-mm interval. For each Z_{org} , the absorber depth Z_r was reconstructed by the two methods [Eq. (9) and Eq. (10)], respectively.

2.4.2 Experiment with pork

We chose fat peeled off from fresh pork as experimental material. Two pieces of fat were chopped into a 100×100 -mm area and 20 mm in thickness. Absorbers (pork muscle and an 8-mm ball) were sandwiched into the two pieces of fat. Glass plates were used to flatten the fat during the process of imaging.

The black ball (8 mm in diameter) was put into the fat at the position (15,30,20) (units are millimeters). Two pieces of muscle were put into the fat. They were both 3-mm thick but of different sizes. The large one is 20×15 mm, in the position (22,27,20), and the smaller one is 10×10 mm, in the position (37,25,20), as shown in Table 3.

3 Results

3.1 Experiments with Intralipid

The reconstruction coordinates of the single absorber experiments are shown in Table 1. Experiment 2 has the largest error in reconstruction coordinate z since the absorber is the farthest from the surface of the solution among the three experiments. Figures 5 and 6 show the combined image and the deblurred image of experiments 2 and 3. The circle in Fig. 5 and the white rectangle in Fig. 6 show the real position and outline of the absorber. The prototype cannot only locate the absorber in Intralipid clearly, but can also estimate the size of the absorber. An absorber as small as a 5-mm-long cylinder can be detected, although the shadow does not look like the absorber.

Table 2 shows the experimental results from an absorber pair. It is difficult to distinguish the two absorbers. Our algorithm gives the coordinates of one absorption peak, which is the middle point of the absorber pair. Figures 7 and 8 show the images of experiments 4 and 5. After the images were deblurred, in Fig. 7 the two absorbers could be distinguished

Table 3 Experiments of absorbers in fat (units are millimeters).

No.	Absorber	Real Coordinates (X, Y, Z)	Distance to the Surface	Reconstruction Coordinates (X_r, Y_r, Z_r)	Error (x, y, z)
6	8-mm ball	(15,30,20)	20	(14.8,29.4,17.9)	(0.2,0.6,2.1)
7	20×15 muscle	(22,27,20)	20	(24.0,27.2,24.8)	(2,0.2,4.8)
	10×10 muscle	(37,25,20)	20	—	—

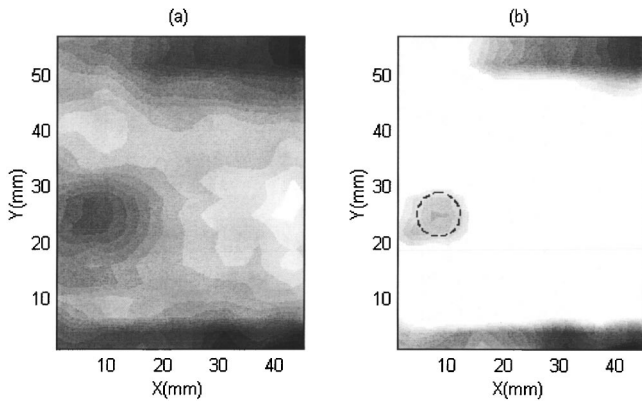


Fig. 5 Images of experiment 2: (a) combined image and (b) deblurred image.

and their size could be estimated. The gray-scale values of the two absorbers are not the same in Fig. 7; this may be due to the mismatch of sources and detectors. In Fig. 8, the two absorbers have one merged shadow. Comparing the images of experiment 5 with experiment 4, we found that the shadows of the absorbers near to the surface are clearer than those farther from the surface.

Figure 9 shows the comparison of the two methods (the straight line versus the S-shaped MPDP). The horizontal axis represents the real depth (Z_{org}) of the absorber. The vertical axis represents the reconstruction depth Z_r . The depth calculated from Eq. (9) is represented by “+” and the depth calculated from Eq. (10) is represented by “○.” The straight line is the ideal reconstruction. Marker “○” is closer to the straight line than marker “+.” This means that the MPDP in the S shape is a better description of the DPDW than the straight line.

3.2 Experiment with Pork

Table 3 shows the experiments of absorbers in fat. As shown in Fig. 10, the 8-mm black ball in fat is very clear. Figure 11 shows the two pieces of muscle in fat. The reconstruction result gives one absorption peak, which points to the larger piece of muscle. After the images are deblurred, the shadows of the two pieces of muscle are distinguishable. This result is

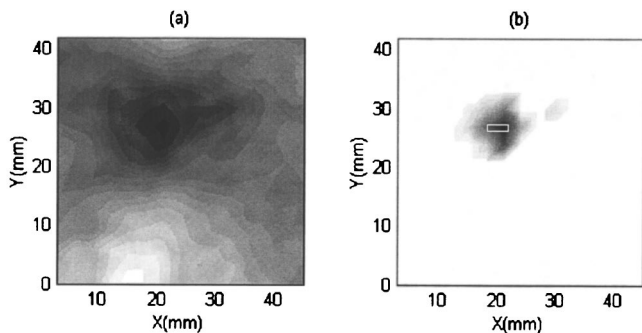


Fig. 6 Images of experiment 3: (a) combined image and (b) deblurred image.

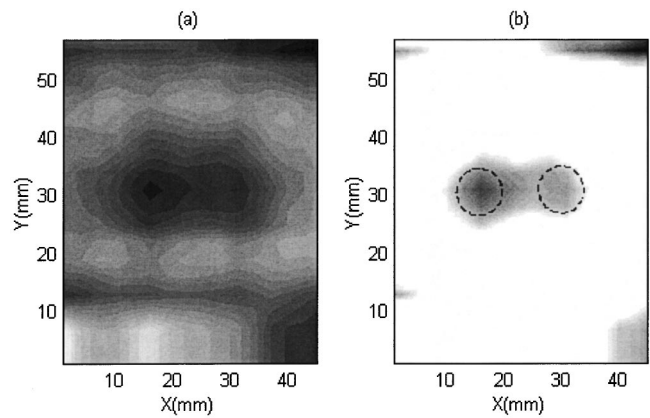


Fig. 7 Images of experiment 4: (a) combined image and (b) deblurred image.

encouraging, for the absorption coefficients of muscle and fat are similar, while the distance between the edges of the two pieces of muscle is only 2 to 3 mm.

4 Discussion

In this paper, we proposed a new description of the MPDP, i.e., in the steady state, which is an alternative description of the most probable trajectory in the TD. We demonstrated the usefulness of the MPDP in 3-D localization of an absorber in a slab. Nonetheless, this concept can be applied in a wide variety of situations. One can employ this method to better configure light sources and detectors, to determine whether the transmission mode or the reflection mode is more appropriate for a given problem, to apply to a multiple-frequency system, and so on. The use of back projection with the MPDP will be a direction of our future study. At the least, images generated in this simple way can act as a good initial solution for iterative algorithms.

In the paper, the MPDP was derived in a 2-D situation and only two boundaries were considered. This might cause some inaccuracy, especially when the MPDP was used in a finite-size phantom or in detection of breast cancer. However, our experiments implemented with a finite-size phantom, showed

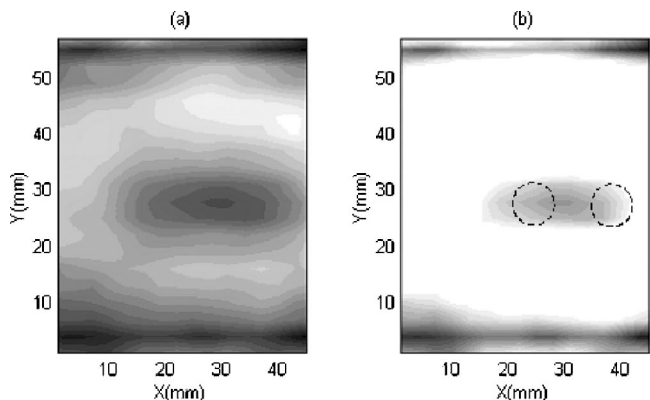


Fig. 8 Images of experiment 5: (a) combined image and (b) deblurred image.

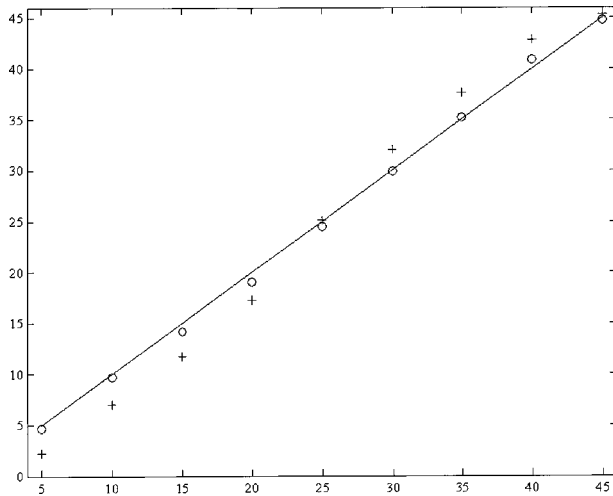


Fig. 9 Comparison of the two different methods.

that the errors were not significant. The MPDP in three dimensions with all boundary conditions should be developed in a coming study.

Our system is capable of imaging turbid media, locating absorbers, and deblurring images. Absorbers 8 mm in diameter can be detected reliably and located accurately. Our localization method, based on the theory of the MPDP, is effective. After the image is deblurred, the size and shape of the absorber can be seen from the image. These are useful in the early detection of breast cancer.

When two absorbers are close to each other, it is difficult to distinguish them, especially when they are deep in tissue. Only their common outline and their center can be found. Reducing the distance between the two detectors and the diameter of fiber bundles will be helpful in improving the resolution.

This method does not consider the shape of breasts, which may cause some errors in clinical study. During clinical experiments, two parallel glass plates will press the breasts. This may be helpful to reduce the error caused by the irregular shape.

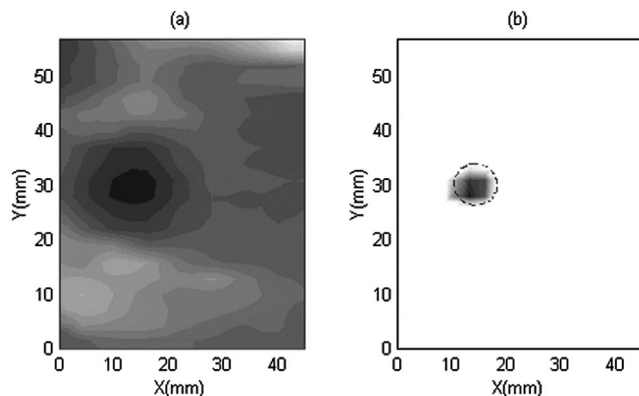


Fig. 10 Images of experiment 6: (a) combined image and (b) deblurred image.

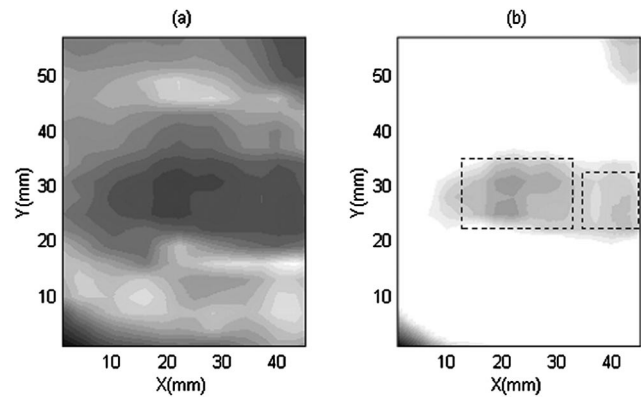


Fig. 11 Images of experiment 7: (a) combined image and (b) deblurred image.

5 Conclusions

In this paper, we proposed the theory of the MPDP of photon in turbid media. A 3-D localization method based on the MPDP theory was also developed to locate absorbers in a slab. To implement the method, a breast cancer detection prototype was designed and assembled in our lab. The phantom experiments gave encouraging results and validated both the prototype and the method. The new 3-D localization method based on the proposed MPDP in the FD can be used to obtain higher accuracy in localizing absorbers embedded in a homogeneous background.

Acknowledgment

This work is supported by the National Natural Science Foundation of China and the Innovation Foundation of PhD Candidates at Tsinghua University.

References

1. D. A. Boas, M. A. O'Leary, B. Chance, and A. G. Yodh, "Scattering of diffuse photon density waves by spherical inhomogeneities with turbid media: analytic solution and applications," *Proc. Natl. Acad. Sci. U.S.A.* **91**, 4887–4891 (1994).
2. M. A. O'Leary, D. A. Boas, B. Chance, and A. G. Yodh, "Experimental images of heterogeneous turbid media by frequency-domain diffusing-photon tomography," *Opt. Lett.* **20**, 426–428 (1995).
3. K. D. Paulsen and H. Jiang, "Enhanced frequency-domain optical image reconstruction in tissues through total-variation minimization," *Appl. Opt.* **35**, 3447–3458 (1996).
4. H. Jiang, K. D. Paulsen, U. L. Osterberg, B. W. Pogue, and M. S. Patterson, "Simultaneous reconstruction of optical absorption and scattering maps in turbid media from near-infrared frequency-domain data," *Opt. Lett.* **20**, 2128–2130 (1995).
5. H. Jiang, K. D. Paulsen, and U. L. Osterberg, "Optical image reconstruction using frequency-domain data: simulations and experiments," *J. Opt. Soc. Am. A* **13**, 253–266 (1996).
6. S. A. Walker, S. Fantini, and E. Gratton, "Image reconstruction by backprojection from frequency-domain optical measurements in high scattering media," *Appl. Opt.* **36**, 170–179 (1997).
7. H. Wabnitz and H. Rinneberg, "Imaging in turbid media by photon density waves: spatial resolution and scaling relations," *Appl. Opt.* **36**, 64–74 (1997).
8. S. Fantini, S. A. Walker, M. A. Franceschini, M. Kaschke, P. M. Schlag, and K. T. Moesta, "Assessment of the size, position, and optical properties of breast tumors in vivo by noninvasive optical methods," *Appl. Opt.* **37**, 1982–1988 (1998).
9. L. T. Perelman, J. Winn, J. Wu, R. R. Dasari, and M. S. Feld, "Photon migration of near-diffusive photons in turbid media: a Lagrangian-based approach," *J. Opt. Soc. Am. A* **14**, 224–229 (1997).

10. L. T. Perelman, J. Wu, Y. Wang, I. Itzkan, R. R. Dasari, and M. S. Feld, "Time-dependent photon migration using path integrals," *Phys. Rev. E* **51**(6), 6134–6141 (1995).
11. L. T. Perelman, J. Wu, I. Itzkan, and M. S. Feld, "Photon migration in turbid media using path integrals," *Phys. Rev. Lett.* **72**, 1341–1344 (1994).
12. V. Tuchin, *Tissue Optics: Light Scattering Methods and Instruments for Medical Diagnosis*, Tutorial Texts in Optical Engineering, Vol. TT38, SPIE Press, Bellingham, WA (2000).
13. S. Arridge and J. C. Hebden, "Optical imaging in medicine: II. Modelling and reconstruction," *Phys. Med. Biol.* **42**, 814–853 (1997).
14. G. I. Bell and S. Glasstone, "Solution of the transport equation by multigroup methods," Chap. 4 in *Nuclear Reactor Theory*, pp. 175–181, Van Nostrand Reinhold, New York (1970).
15. J. B. Fishkin and E. Gratton, "Propagation of photon-density waves in strongly scattering media containing an absorbing semi-infinite plane bounded by a straight edge," *J. Opt. Soc. Am. A* **10**(1), 127–140 (1993).
16. R. C. Haskell, L. O. Svaasand, T. T. Tsay, T. C. Feng, M. S. McAdams, and B. J. Tromberg, "Boundary conditions for the diffusion equation in radiative transfer," *J. Opt. Soc. Am. A* **11**(10), 2727–2741 (1994).
17. N. G. Chen and J. Bai, "Monte Carlo approach to modeling of boundary conditions for the diffusion equation," *Phys. Rev. Lett.* **80**(24), 5321–5324 (1998).
18. M. A. Franceschini, K. T. Moesta, S. Fantini, G. Gaida, E. Gratton, H. Jess, W. W. Mantulin, M. Seeber, P. M. Schlag, and M. Kaschke, "Frequency-domain techniques enhance optical mammography: initial clinical results," *Proc. Natl. Acad. Sci. U.S.A.* **94**, 6468–6473 (1997).